Multi-target Optimal Control Problems for a Tentacle-like Soft Manipulator

Simone Cacace[1], Anna Chiara Lai[2] [a] and Paola Loreti[2]

[1]*Dipartimento di Matematica e Fisica, Università degli Studi Roma Tre, Largo S. Murialdo, 1, 00154 Roma, Italy*

[2]*Dipartimento di Scienze di Base e Applicate per l'Ingegneria, Sapienza Università di Roma, Via A. Scarpa, 16, 00161 Roma, Italy*

Keywords: Soft Manipulators, Control Strategies, Reachability, Multi-target Problems, Optimal Control.

Abstract: We investigate the optimality of the configurations of a tentacle-like soft manipulator ensuring the contact with a target object, while avoiding an obstacle. The main novelty consists in treating the contact sub-region of the manipulator as an unknown of the problem and, at the same time, in allowing the target to be disconnected. We set the optimization problem in full generality, then we focus on the case of a multi-target problem, in which the goal is to simultaneously reach a finite set of points. Numerical simulations complete the paper.

1 INTRODUCTION

In this paper, we investigate the optimality of the configurations of a tentacle-like soft manipulator ensuring the simultaneous contact with several, disconnected targets, and obstacle avoidance. In (Cacace et al., 2020a), we introduced a control model for a soft manipulator, modelled as an inextensible string subject to a bending moment, a curvature constraint and a pointwise curvature control. The dynamics of the manipulator was then studied in an optimal control theoretic perspective, with the purpose of characterizing optimal control strategies for several tasks, including optimal reachability problems (Cacace et al., 2019a), obstacle avoidance (Cacace et al., 2020b; Cacace et al., 2021) and grasping problems (Cacace et al., 2019b).

In particular, in (Cacace et al., 2019b) it was addressed the problem, in a stationary setting, to touch the boundary of a target object with a prescribed portion of the manipulator, while avoiding interpenetration and minimizing a quadratic cost on the controls. Here we move a step forward in this direction, letting the manipulator touch some fixed points on the boundary of the target object using contact points which optimize a given integral cost. Hence the main novelty consists in treating the contact sub-region of the manipulator as an unknown of the problem and, at the same time, in allowing the target to be discon-

nected. For instance, if the target is a set of points (possibly on the boundary of the obstacle), we are looking for an optimal, obstacle avoiding configuration of the manipulator which "interpolates" the set of the target points. We numerically solve several optimal problems in this scenario, whereas the theoretical framework is set in full generality.

The paper is organized as follows. In Section 2, we recall our model for tentacle-like soft manipulators and the associated equilibria. In Section 3, we present the multi-target optimal control problem, the corresponding optimality system, and an iterative method for its solution. In Section 4, we discuss the numerical approximation and implementation of the proposed algorithm, then we show the results of the numerical experiments. Finally, in Section 5, we present our conclusions.

We refer to (Michalak et al., 2014; Rus and Tolley, 2015; Laschi and Cianchetti, 2014; George Thuruthel et al., 2018) and the reference therein for a general introduction on soft robotics and related motion planning problems. The paper (Hughes et al., 2016) surveys grasping problems for soft-manipulators, where we refer to the papers (Bobrow et al., 1983; Wang et al., 2016) for an optimal control theoretic approach to constrained reachability problems. The model discussed here was earlier introduced in (Cacace et al., 2020a), related references include (Jones and Walker, 2006; Kang et al., 2011; Lai and Loreti, 2014; Lai et al., 2016; Laschi et al., 2012).

---

[a] https://orcid.org/0000-0003-2096-6753

2 MODELING A TENTACLE-LIKE SOFT-MANIPULATOR

In (Cacace et al., 2020a), we introduced a control model for a soft manipulator inspired by the morphology of an octopus tentacle. We considered a three-dimensional body with an axial symmetry, a non-uniform thickness and a fixed endpoint. We assumed the device to be subject to an inextesibility constraint (preventing longitudinal stretching) and to a bending moment, constraint and control. The bending of the device is hence opposed by a natural resistance, represented by the bending moment; the bending is however bounded by a non-uniform threshold represented by the bending constraint and, finally, the controller can force the bending pointwise. Exploting axial symmetry, we restricted the investigation to the symmetry axis, by ending up in a planar dynamics and an unidimensional problem. From a physical point of view, such an axis is modelled as an inextensible string, whose mass represents the mass of the whole manipulator. Also bending constraints (and controls) of the manipulator are projected on the axis: they are identified by suitably weighted curvature constraints, see (Cacace et al., 2019a) for details on this projection. In particular, the bending constraint is translated into forcing the curvature of the axis under a fixed (non-uniform) threshold ω; the bending control is translated into forcing the signed curvature to the quantity ωu, where $u \in [-1,1]$ is the control map. Curvature constraints and control, as well as the bending moment, are embedded via penalization, whereas the inextensibility constraint is exact.

The unknowns of our problem are the curve $q(s,t): [0,1] \times \mathbb{R}^+ \to \mathbb{R}^2$ parametrizing the symmetry axis of the manipulator in arclength coordinates, and the associated inextensibility multiplier $\sigma(s,t) \in \mathbb{R}$. We denote by q_s, q_{ss}, q_{tt} partial derivatives in space and time respectively. The quantity $|q_{ss}|$ represents the curvature of q, whereas the product $q_s \times q_{ss} := q_s \cdot q_{ss}^\perp$ represents the signed curvature, where the symbol $q_{ss}^\perp$ denotes the counter-clockwise orthogonal vector to q_{ss}. With these notations, we summarize the constraints described above in Table 1, that we recall from (Cacace et al., 2019a). We refer to Figure 1-(b) – Figure 6-(b) for an example of the curvature threshold ω and some (optimal) control functions u.

Then, the evolution of q (and of the corresponding inextensibility multiplier $\sigma: [0,1] \times [0,+\infty) \to \mathbb{R}$) is obtained, via the least action principle, by the following Lagrangian:

Table 1: Exact constraint equations and related elastic potentials derived from penalty method. The functions ν and μ represent non-uniform elastic constants.

Constraint	Constraint equation	Penalization elastic potential
Inextensibility	$|q_s| = 1$	None
Curvature	$|q_{ss}| \leq \omega$	$\nu(|q_{ss}|^2 - \omega^2)_+^2$
Control	$q_s \times q_{ss} = \omega u$	$\mu(\omega u - q_s \times q_{ss})^2$

$$
\mathcal{L}(q,\sigma) := \int_0^1 \Big(\underbrace{\frac{1}{2}\rho|q_t|^2}_{\text{kinetic energy}} - \underbrace{\frac{1}{2}\sigma(|q_s|^2-1)}_{\text{inextensibility constr.}}
$$
$$
- \underbrace{\frac{1}{4}\nu\left(|q_{ss}|^2-\omega^2\right)_+^2}_{\text{curvature constr.}} - \underbrace{\frac{1}{2}\varepsilon|q_{ss}|^2}_{\text{bending moment}}
$$
$$
- \underbrace{\frac{1}{2}\mu(\omega u - q_s \times q_{ss})^2}_{\text{curvature control}} \Big) ds,
$$

Equations of motions are explicitly derived in (Cacace et al., 2020a), to which we also refer for a more rigorous justification of the definition of $\mathcal{L}$. Here we are most interested in recalling the stationary configurations associated to above Lagrangian. Assuming the technical condition $\mu(1) = \mu_s(1) = 0$, the shape of the manipulator at the equilibrium is the solution q of the following second order controlled ODE:

$$
\begin{cases}
q_{ss} = \bar{\omega} u q_s^\perp & \text{in } (0,1) \\
|q_s|^2 = 1 & \text{in } (0,1) \\
q(0) = (0,0) \\
q_s(0) = (0,-1).
\end{cases} \tag{1}
$$

where $\bar{\omega} := \mu\omega/(\mu+\varepsilon)$ is the effective threshold due to the competition between the bending moment and the curvature control.

3 THE MULTI-TARGET OPTIMAL CONTROL PROBLEM

Let Ω_0 be an open subset of $\mathbb{R}^2$ representing the obstacle, and let $\Omega_1 \subset \mathbb{R}^2 \setminus \Omega_0$ be a closed target set – we also allow the case $\Omega_1 \subset \partial\Omega_0$. We consider the following optimal control problem

$$
\min \mathcal{G}, \quad \text{subject to (1) and to } |u| \leq 1, \tag{2}
$$

where

$$
\mathcal{G}(q,u) := \frac{1}{2}\int_0^1 u^2 ds
$$
$$
+ \frac{1}{2\tau_0}\int_0^1 W_0(q(s))ds + \frac{1}{2\tau_1}\int_0^1 W_1(q(s))\mu_0(s)ds \tag{3}
$$

is the cost functional for the multi-target problem, for some positive penalty parameters τ_0 and τ_1. The first integral term of $\mathcal{G}$ is a quadratic cost on the controls, which is related via (1) to the curvature of the manipulator. The potential $W_0 : \mathbb{R}^2 \to \mathbb{R}$ is a positive function supported in Ω_0, and acting as an obstacle, i.e. forcing all the points of the manipulator to move outside Ω_0. Similarly, $W_1 : \mathbb{R}^2 \to \mathbb{R}$ is a positive potential supported in the complement Ω_1^c, so that the third term in (3) penalizes the distance from the target Ω_1, attracting points according to μ_0, a non negative weight describing which parts of the manipulator are preferred for touching the target.

In (Cacace et al., 2019b; Cacace et al., 2021), problem (2) was investigated and then numerically solved when $\Omega_1 = \partial\Omega_0$ and μ_0 is prescribed. Here, we move further, by considering $\Omega_1 := \{p_1, \ldots, p_N\}$, namely a set of N fixed points, possibly located on $\partial\Omega_0$. Moreover, we introduce N additional unknowns $S = \{s_1, \ldots, s_N\} \in I_\gamma := [\gamma, 1-\gamma]$, i.e. real numbers belonging, for some small parameter $\gamma > 0$, to the interior of the parametrization interval of the manipulator, and we assume that $\mu_0(s) = \sum_{i=1}^N \delta_{s_i}(s)$ is a Dirac measure concentrated on S. With these choices, the functional $\mathcal{G}$ in (3) takes the form

$$
\begin{aligned}
\mathcal{G}(q,S) := &\frac{1}{2}\int_0^1 \frac{1}{\bar{\omega}^2(s)}|q_{ss}|^2 ds \\
&+ \frac{1}{2\tau_0}\int_0^1 W_0(q(s))ds + \frac{1}{2\tau_1}\sum_{i=1}^N |q(s_i) - p_i|^2,
\end{aligned}
\tag{4}
$$

where we used (1) to replace the control term by the curvature of the manipulator, weighted by $\bar{\omega}$. Then, the optimal control problem (2) now consists in minimizing $\mathcal{G}$ with respect to q and S, subject to the constraints $q(0) = (0,0)$, $q_s(0) = (0,-1)$, $|q_s(s)|^2 = 1$, $|q_{ss}| \leq \bar{\omega}$ for $s \in (0,1)$ and $s_i \in I_\gamma$ for $i = 1, \ldots, N$.

To obtain necessary optimality conditions, we first relax the inequality constraint on the curvature $|q_{ss}| \leq \bar{\omega}$, by introducing a so called *slack variable*, namely we impose the equivalent (and simpler to treat) equality constraint $|q_{ss}|^2 - \bar{\omega}^2 + z = 0$ with $z \geq 0$. Then, we introduce the following augmented Lagrangian

$$
\begin{aligned}
\mathcal{L}(q,\sigma,S,z,\lambda) := &\mathcal{G}(q,S) + \frac{1}{2}\int_0^1 \sigma(|q_s|^2 - 1)ds \\
&+ \frac{1}{2}\int_0^1 \lambda(|q_{ss}|^2 - \bar{\omega}^2 + z)ds \\
&+ \frac{1}{4\rho_\lambda}\int_0^1 (|q_{ss}|^2 - \bar{\omega}^2 + z)^2 ds,
\end{aligned}
\tag{5}
$$

where σ is again an exact Lagrange multiplier for the inextensibility constraint, while λ and $\rho_\lambda > 0$ are respectively the multiplier and penalty parameter related to the relaxed constraint on the curvature. In this setting, our optimal control problem

is equivalent to the optimization of $\mathcal{L}$, which can be performed employing the method of multipliers ((Hestenes, 1969; Powell, 1969), see also (Christian Kanzow and Wachsmuth, 2018) and the references therein for the infinite-dimensional case), iterating on $k \geq 0$ up to convergence

$$
\begin{cases}
(\tilde{q}^{(k+1)}, \tilde{\sigma}^{(k+1)}, \tilde{S}^{(k+1)}, \tilde{z}^{(k+1)}) = \\
\quad \underset{\substack{q,\sigma \\ S \in I_\gamma, z \geq 0}}{\arg\min} \ \mathcal{L}(q,\sigma,S,z,\lambda^{(k)}) \\
\lambda^{(k+1)} = \lambda^{(k)} + \dfrac{1}{\rho_\lambda}(|\tilde{q}_{ss}^{(k+1)}|^2 - \bar{\omega}^2 + \tilde{z}^{(k+1)}).
\end{cases}
\tag{6}
$$

Here, the dependence on z can be dropped. Indeed, the optimization with respect to $z \geq 0$ yields the following variational inequality

$$
\int_0^1 (\lambda^{(k)}\rho_\lambda + |q_{ss}|^2 - \bar{\omega}^2 + z)(v - z)ds \geq 0, \quad \forall v \geq 0,
$$

and its solution is given pointwise by

$$
z = z(q, \lambda^{(k)}) = \max\left\{ -\lambda^{(k)}\rho_\lambda - |q_{ss}|^2 + \bar{\omega}^2, 0 \right\}.
$$

This allows to reduce the update formula for the multiplier in (6) to

$$
\lambda^{(k+1)} = \max\left\{ \lambda^{(k)} + \frac{1}{\rho_\lambda}(|\tilde{q}_{ss}^{(k+1)}|^2 - \bar{\omega}^2), 0 \right\}.
\tag{7}
$$

On the other hand, the solution $(\tilde{q}^{(k+1)}, \tilde{\sigma}^{(k+1)}, \tilde{S}^{(k+1)})$ of the optimization sub-problem for the reduced Lagrangian

$$
\mathcal{L}^{(k)}(q,\sigma,S) := \mathcal{L}(q,\sigma,S,z(q,\lambda^{(k)}),\lambda^{(k)})
\tag{8}
$$

satisfies the following optimality system

$$
\begin{cases}
\left(\Lambda^{(k)}(q_{ss})q_{ss}\right)_{ss} - (\sigma q_s)_s \\
\quad + \frac{1}{\tau_0}\nabla W_0(q(s)) \\
\quad + \frac{1}{\tau_1}\sum_{i=1}^N (q(s) - p_i)\delta_{s_i}(s) = 0 & \text{in } (0,1) \\
|q_s|^2 = 1 & \text{in } (0,1) \\
\frac{1}{\tau_1}(q(s_i) - p_i)\cdot q_s(s_i)(w_i - s_i) \geq 0, & \forall w_i \in I_\gamma \\
& i = 1,\ldots,N \\
q(0) = 0, \quad q_s(0) = (0,-1) \\
q_{ss}(1) = 0, \quad q_{sss}(1) = 0, \\
\sigma(1) = 0,
\end{cases}
\tag{9}
$$

with

$$
\Lambda^{(k)}(q_{ss}) := \frac{1}{\bar{\omega}^2} + \max\left\{ \lambda^{(k)} + \frac{1}{\rho_\lambda}(|q_{ss}|^2 - \bar{\omega}^2), 0 \right\}.
$$

The first equation and the boundary conditions in (9) emerge from the optimization of $\mathcal{L}^{(k)}$ with respect

to q. We refer to (Cacace et al., 2020a) for details, and we remark that the novelty in this paper is the obstacle repulsion –which is provided by the gradient of the potential W_0– and the contact set S appearing in the last term of the equation, a force field whose source points attract single particles of the manipulator.

The second equation is the inextensibility constraint, recovered by the optimization of $\mathcal{L}^{(k)}$ with respect to σ.

Finally, the optimization with respect to $s_i \in I_\gamma$ for $i = 1, \ldots, N$ provides the variational inequalities in (9). Note that, if for some i the optimal s_i falls in the interior of I_γ, then

$$\frac{1}{\tau_1}(q(s_i) - p_i) \cdot q_s(s_i) = 0, \qquad i = 1, \ldots, N. \quad (10)$$

From a geometric point of view, this condition is clearly satisfied, as $\tau_1 \to 0$, if s_i realizes a perfect contact $q(s_i) = p_i$, but since the contact is imposed via penalization with $\tau_1 << 1$, condition (10) weakens in requesting a null projection of $(q(s_i) - p_i)$ on the tangent vector $q_s(s_i)$.

We now employ a projected gradient descent method for the approximation of the solution of (9). To this end, we collect the partial Fréchet derivatives of $\mathcal{L}^{(k)}$ in

$$\mathcal{L}'^{(k)}(q, \sigma, S) = \begin{pmatrix} \left(\Lambda^{(k)}(q_{ss})q_{ss}\right)_{ss} - (\sigma q_s)_s \\ + \frac{1}{\tau_0}\nabla W_0(q(s)) \\ + \frac{1}{\tau_1}\sum_{i=1}^N (q(s) - p_i)\delta_{s_i}(s) \\ \frac{1}{2}(|q_s|^2 - 1) \\ \frac{1}{\tau_1}(q(s_1) - p_1) \cdot q_s(s_1) \\ \vdots \\ \frac{1}{\tau_1}(q(s_N) - p_N) \cdot q_s(s_N) \end{pmatrix}, \quad (11)$$

where the last N entries correspond to the unconstrained cases (10) for the variational inequalities in (9).

Then, given an initial guess $(q^{(0)}, \sigma^{(0)}, S^{(0)})$, we iterate on $n \geq 0$ up to convergence

$$\begin{cases} \begin{pmatrix} q^{(n+1)} \\ \sigma^{(n+1)} \\ \bar{s}^{(n+1)} \end{pmatrix} = \begin{pmatrix} q^{(n)} \\ \sigma^{(n)} \\ S^{(n)} \end{pmatrix} - \alpha \mathcal{L}'^{(k)}(q^{(n)}, \sigma^{(n)}, S^{(n)}), \\ \\ S^{(n+1)} = \Pi_{I_\gamma}\left(\bar{s}^{(n+1)}\right), \end{cases} \quad (12)$$

where $\alpha > 0$ is the step size and

$$\Pi_{I_\gamma}(\cdot) = \min\{\max\{\cdot, \gamma\}, 1 - \gamma\}$$

is the component-wise projection on I_γ ensuring a feasible contact set at each iteration.

We conclude this section by remarking that, at least at a formal level, the presented analysis has been carried on in an infinite-dimensional setting, but its rigorous justification and the proof of convergence results for both the method of multipliers and the projected gradient descent method is a very delicate task which is still under development.

4 NUMERICAL APPROXIMATION AND SIMULATIONS

We briefly discuss the relevant steps for the approximation of the multi-target problem, then we build our algorithm for an actual implementation. Finally, we present the results for several numerical experiments, showing the effectiveness of the proposed approach.

After introducing a uniform grid on the parametrization interval of the manipulator, the discretization of the derivatives appearing in (11) is performed using standard finite differences, while the boundary conditions in (9) can be handled adding suitable ghost nodes at the end points. Moreover, we observe that the contact values $S = \{s_1, \ldots, s_N\}$ need not to be discretization nodes, hence the corresponding contact points $q(s_1), \ldots, q(s_N)$ in (11) are reconstructed via linear interpolation of neighboring grid nodes. We also use a rectangular quadrature rule to evaluate all the integrals in the Lagrangian $\mathcal{L}^{(k)}$ (see (8), (5) and (4)). Finally, the penalty parameters τ_0, τ_1 and ρ_λ must be chosen very small in order to enforce, respectively, the obstacle avoidance, the contact with the target points and the curvature constraint. Here we use a continuation method to slowly decrease these parameters, by means of a scaling factor $\chi < 1$. For simplicity, we embed this update in the iteration step for the method of multipliers (6).

We have to remark that, despite its straightforward implementation, the gradient descent method is known to suffer a severe restriction on the step size α, hence it requires a very large number of iterations to reach convergence. Computational efforts can be mitigated introducing more sophisticated techniques, such as an inexact line-search strategy based on the Armijo–Goldstein condition to obtain an almost optimal α. Alternatively, we can directly apply a Newton method to the problem $\mathcal{L}'^{(k)} = 0$, but it requires the computation of the second Fréchet derivative $\mathcal{L}''^{(k)}$, which is very involved in the present setting. This goes beyond the scope of the paper and we omit the details.

We finally build the following algorithm.

Algorithm 1.

1: Assign the obstacle Ω_0, the potential W_0, the curvature threshold $\bar{\omega}$, the N target points $\{p_1, \ldots, p_N\} \in \partial \Omega_0$, the interval I_γ, an initial guess $(q^\sharp, \sigma^\sharp, S^\sharp)$, initial penalty parameters $\tau_0, \tau_1, \rho_\lambda$, a step size α, a scaling factor $\chi < 1$ and a tolerance $tol > 0$.
2: Set $k \leftarrow 0$
3: Set $(\tilde{q}^{(k)}, \tilde{\sigma}^{(k)}, \tilde{S}^{(k)}) \leftarrow (q^\sharp, \sigma^\sharp, S^\sharp)$
4: Compute $\mathcal{L}_{out}^{new} = \mathcal{L}^{(k)}(q^\sharp, \sigma^\sharp, S^\sharp)$
5: Set $\mathcal{L}_{in}^{new} \leftarrow \mathcal{L}_{out}^{new}$
6: **repeat** (Method of multipliers)
7:     Set $n \leftarrow 0$
8:     Set $(q^{(n)}, \sigma^{(n)}, S^{(n)}) \leftarrow (\tilde{q}^{(k)}, \tilde{\sigma}^{(k)}, \tilde{S}^{(k)})$
9:     Set $\mathcal{L}_{out}^{old} \leftarrow \mathcal{L}_{out}^{new}$
10:     **repeat** (Projected gradient descent method)
11:         Set $\mathcal{L}_{in}^{old} \leftarrow \mathcal{L}_{in}^{new}$
12:         Compute $(q^{(n+1)}, \sigma^{(n+1)}, S^{(n+1)})$ using (12)
13:         Compute $\mathcal{L}_{in}^{new} = \mathcal{L}^{(k)}(q^{(n+1)}, \sigma^{(n+1)}, S^{(n+1)})$
14:         Set $n \leftarrow n + 1$
15:     **until** $\left| \mathcal{L}_{in}^{new} - \mathcal{L}_{in}^{old} \right| < tol$
16:     Set $(\tilde{q}^{(k+1)}, \tilde{\sigma}^{(k+1)}, \tilde{S}^{(k+1)}) \leftarrow (q^{(n)}, \sigma^{(n)}, S^{(n)})$
17:     Compute $\lambda^{(k+1)}$ using (7)
18:     Set $\tau_0 \leftarrow \chi \tau_0$
19:     Set $\tau_1 \leftarrow \chi \tau_1$
20:     Set $\rho_\lambda \leftarrow \chi \rho_\lambda$
21:     Set $\mathcal{L}_{out}^{new} \leftarrow \mathcal{L}_{in}^{new}$
22:     Set $k \leftarrow k + 1$
23: **until** $\left| \mathcal{L}_{out}^{new} - \mathcal{L}_{out}^{old} \right| < tol$

Table 2: Obstacle and target settings. $Q_l(c)$ denotes the square of side $l = 0.3$ and center $c = (0.2, -0.3)$.

| Test #	Ω_0	Ω_1
1	$\emptyset$	$\{(0.25, -0.7)\}$
2	$\emptyset$	$\{(0.094, -0.406), (0.094, -0.406)\}$
3	$\emptyset$	$\{(0.05, -0.3), (0.2, -0.45), (0.35, -0.3)\}$
4	$\emptyset$	$\{(0.1, -0.3), (0.2, -0.45), (0.3, -0.3)\}$
5	$\emptyset$	$\{(0.135, -0.3), (0.2, -0.5), (0.265, -0.3)\}$
6	$Q_l(c)$	$\{(0.05, -0.15), (0.05, -0.45), (0.35, -0.45)\}$
7	$Q_l(c)$	$\{(0.05, -0.3), (0.2, -0.45), (0.35, -0.3)\}$

Let us now define the settings for our numerical experiments, summarized in Table 2. We first focus on the case without obstacle, i.e. $\Omega_0 = \emptyset$ and $W_0 \equiv 0$, with a number N of target points between 1 and 3. Then, we consider the case $\Omega_0 = Q_l(c)$ (the square of side l centered at $c \in \mathbb{R}^2$) with $l = 0.3$ and $c = (0.2, -0.3)$. Moreover, we choose $W_0(x) = \left(\frac{l}{2} - \|x - c\|_\infty \right)_+^2$ and $N = 3$ target points on $\partial \Omega_0$ in different configurations. In all the tests we choose the curvature threshold function $\bar{\omega}(s) = \frac{1 - 0.9s}{(1 - 0.9s) + (0.1 - 0.09s)} 2\pi(2 + s^2)$, corresponding to (1) with $\omega(s) = 2\pi(2 + s^2)$, $\mu(s) = 1 - 0.9s$ and $\varepsilon(s) = 0.1 - 0.09s$. We assume that the manipulator has unit length and it is discretized with 201 nodes. We

set $\gamma = \frac{1}{200}$, namely equal to the mesh size, so that the interval I_γ contains all the grid nodes except the end points. As initial guess, we always choose $q^\sharp$ close enough to the target points, whereas $\sigma^\sharp \equiv 0$ and $S^\sharp$ is such that all the starting contact points are equally spaced around the midpoint of the manipulator. Finally, we set the starting penalty parameters $\tau_0 = \tau_1 = \rho_\lambda = 10^{-3}$, while $\alpha = 5 \cdot 10^{-3}$, $\chi = 0.999$ and $tol = 10^{-12}$.

We begin with the simple test of a single target point $p_1 = (0.25, -0.7)$, Test 1. In Figure 1-(a) we show the computed optimal configuration q of the manipulator, the target point (black circle) and the optimal contact point (yellow circle), while Figure 1-(b) represents the corresponding signed curvature (thicker line) as a function of $s \in [0, 1]$, and the thresholds $\pm \bar{\omega}(s)$ (thin lines). Finally, in Figure 1-(c) we show the behavior of the contact value $s_1 \in I_\gamma$ versus the total number of iterations to reach convergence, i.e. accounting for both inner and outer loops in Algorithm 1. We clearly observe the sliding of s_1 toward the free end, and its convergence.

In Test 2, we choose the two target points $p_1 = (0.094, -0.406)$, $p_2 = (0.306, -0.406)$, and we report the results in Figure 2. In particular, we observe the evolution of the contact values s_1 and s_2 in Figure 2-(c): their behavior is similar to the one of the previous test for about the first 10^3 iterations. In this phase the manipulator is attracted and then pinned to the target points, due to the large value of the penalty parameter τ_1. Once the corresponding target term in $\mathcal{L}^{(k)}$ is sufficiently reduced, the optimization proceeds trying to decrease the curvature term. This is done in the remaining iterations, where we observe a further sliding of s_1 and s_2 before the convergence.

We proceed by considering the case of three target points at closer and closer distances, that is Test 3, 4 and 5. Figure 3 shows the results for Test 3, with $p_1 = (0.05, -0.3)$, $p_2 = (0.2, -0.45)$ and $p_3 = (0.35, -0.3)$, while Figure 4 corresponds to Test 4, with $p_1 = (0.1, -0.3)$, $p_2 = (0.2, -0.45)$ and $p_3 = (0.3, -0.3)$. For both configurations, we observe a behavior of the contact values s_1, s_2, s_3 similar to the previous test, but, in the second one, the final sliding phase is much more evident. This is due to the closer distance between p_1 and p_3, forcing the curvature of the manipulator, during the optimization, up to the threshold $\bar{\omega}$ on a large interval. Hence, the optimal solution prefers to retract, adding a double change of sign in the curvature around p_1 and reaching $\bar{\omega}$ on a much smaller interval, see Figure 4-(b) and also Figure 3-(b) for comparison. Finally, Figure 5 corresponds to Test 5 with $p_1 = (0.135, -0.3)$, $p_2 = (0.2, -0.5)$ and $p_3 = (0.265, -0.3)$, which pro-
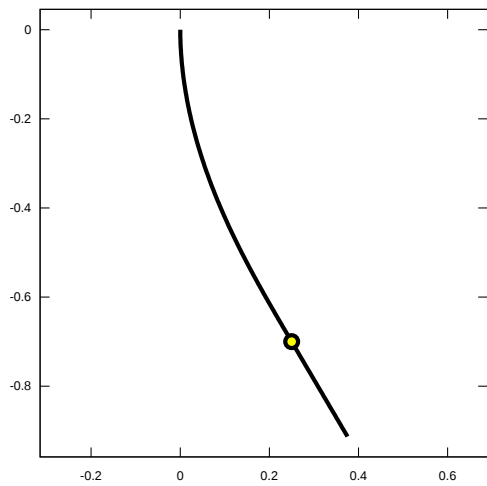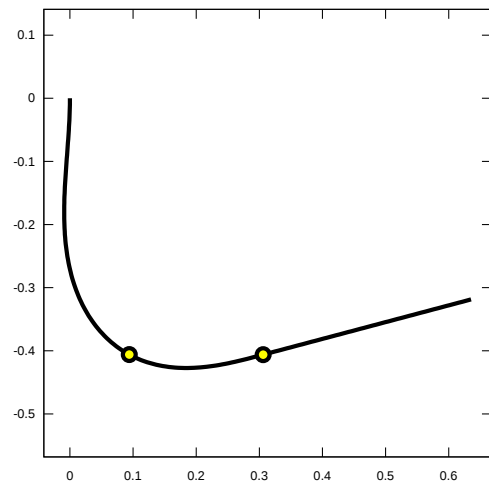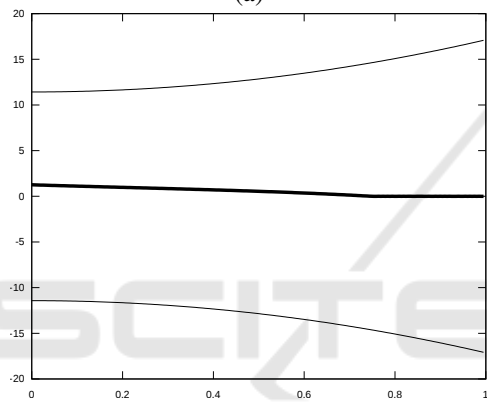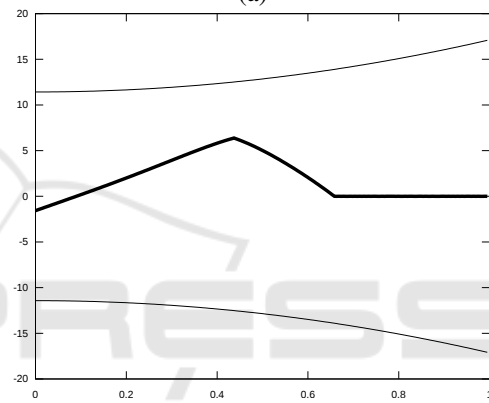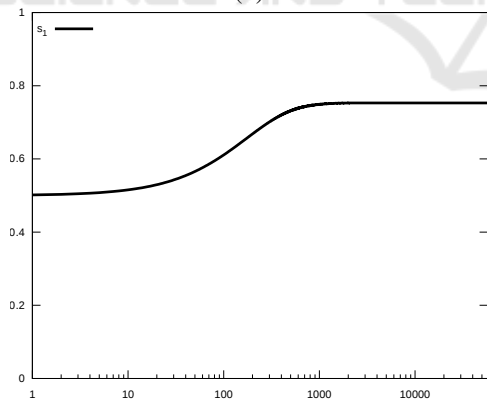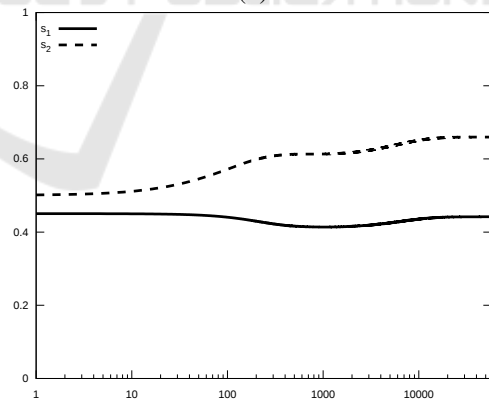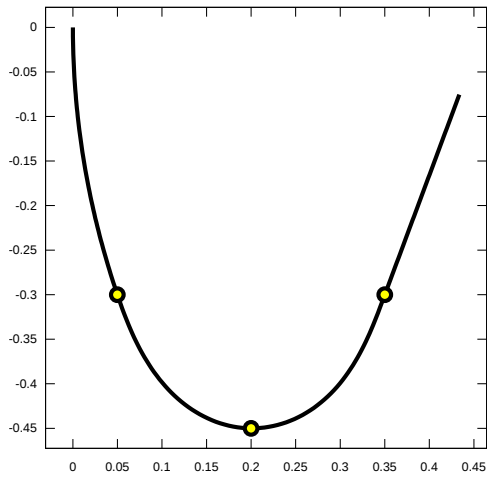
Figure 1: Test 1, optimal configuration (a), optimal curvature (b), and convergence history of the optimal contact value (c).

Figure 2: Test 2, optimal configuration (a), optimal curvature (b), and convergence history of the optimal contact values (c).

vides an even more extreme configuration. Indeed, the requested bending for touching the target points is so high that it is better for the manipulator to retract almost up to its free end, as shown by the large sliding of the contact value s_3 in Figure 5-(c). The op-

timal solution still adds a double change of sign in the curvature around p_1, with larger values (in modulus) in the part preceding p_1, see also Figure 4 for comparison.

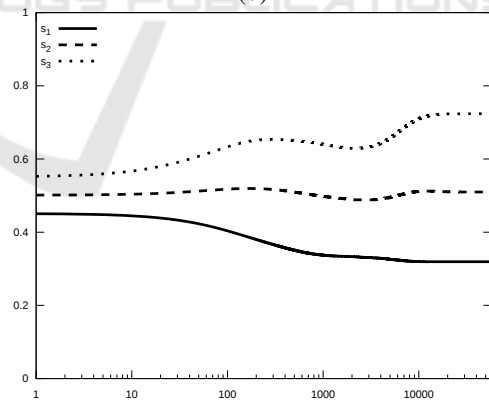We now consider two examples including the square

(a)

(b)
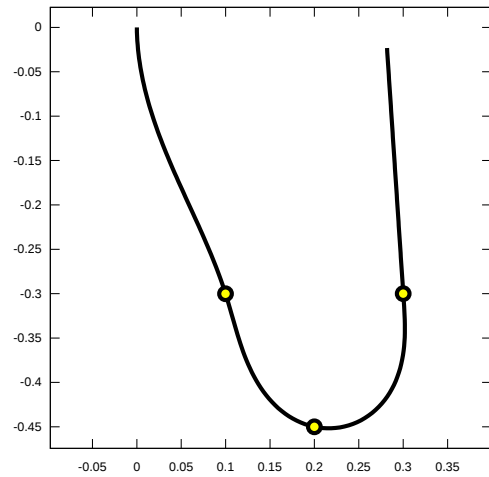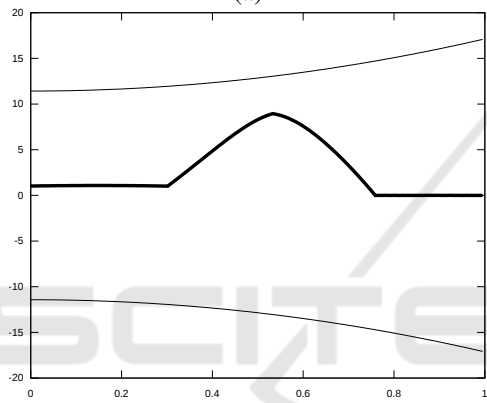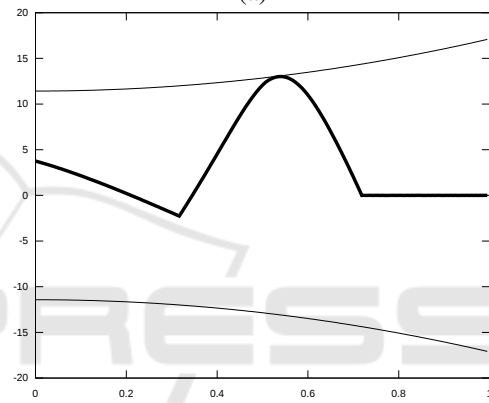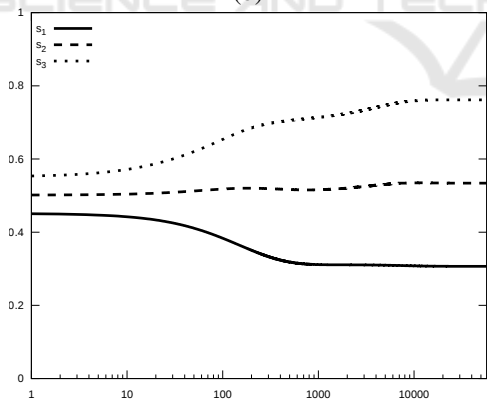
(c)

Figure 3: Test 3, optimal configuration (a), optimal curvature (b), and convergence history of the optimal contact values (c).

(a)

(b)

(c)

Figure 4: Test 4, optimal configuration (a), optimal curvature (b), and convergence history of the optimal contact values (c).

obstacle described above. In Test 6, we choose $p_1 = (0.05, -0.15)$, $p_2 = (0.05, -0.45)$ and $p_3 = (0.35, -0.45)$, namely three vertices of the square, and we show the results in Figure 6. It is worth noting that the manipulator touches the obstacle just at

the target points, but not along the left and bottom sides. The reason is twofold: first, a flat configuration across the corner p_2 would produce a jump in the tangent vector q_s and hence an infinite curvature at p_2; second, the first term in the functional (4), namely the
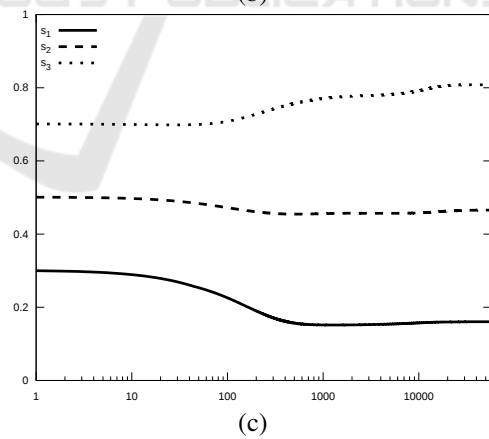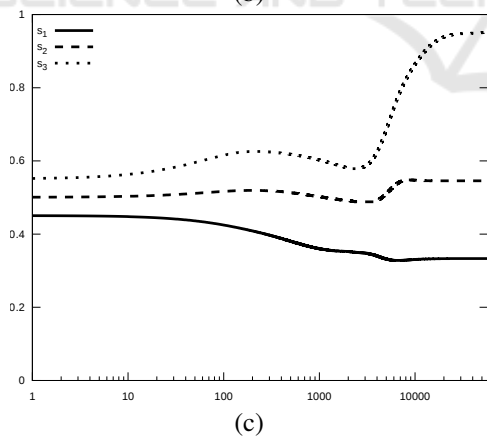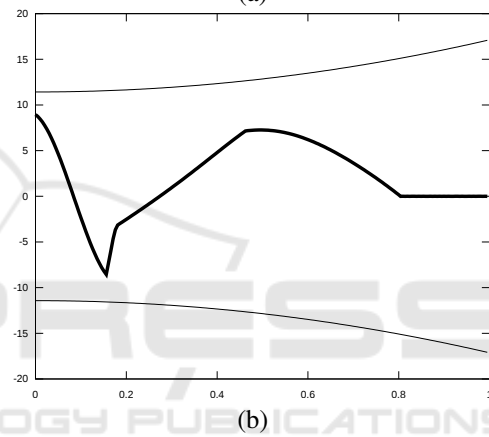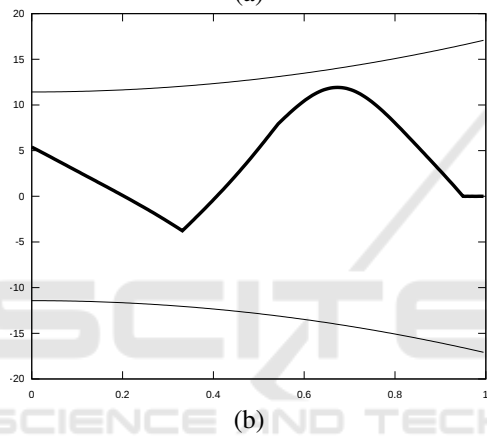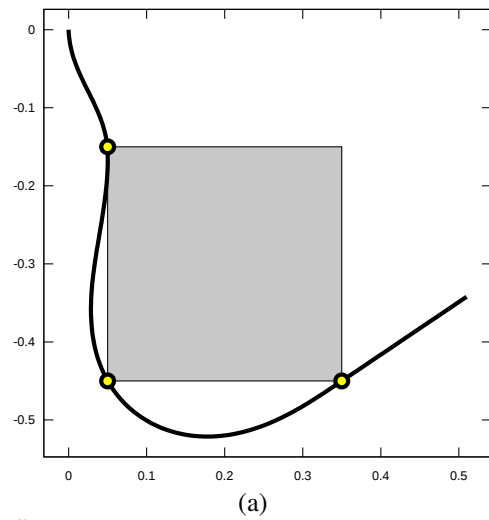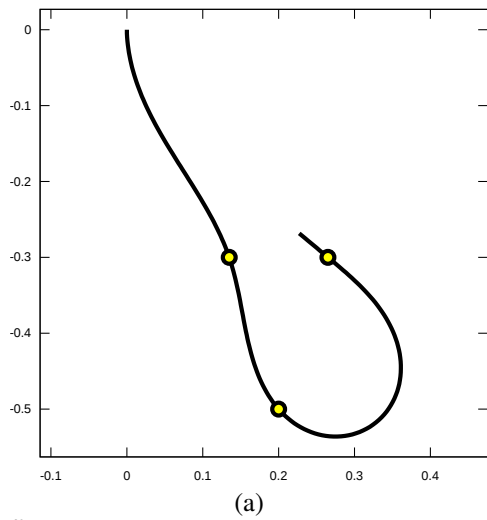
Figure 5: Test 5, optimal configuration (a), optimal curvature (b), and convergence history of the optimal contact values (c).

Figure 6: Test 6, optimal configuration (a), optimal curvature (b), and convergence history of the optimal contact values (c).

squared L^2 norm of the weighted curvature, acts as a regularization. It prevents the curvature to develop jump singularities (or, in other words, it forbids *bang-bang* controls, if we recall that $|q_{ss}| = \bar{\omega}|u|$ by (1)), and it replaces them with suitable continuous transi-

tions. This is more evident in our last and much difficult experiment, Test 7, shown in Figure 7, where the target points $p_1 = (0.05, -0.3)$, $p_2 = (0.2, -0.45)$ and $p_3 = (0.35, -0.3)$ corresponds to the midpoints of three sides of the square. Note also that, in order to

5 CONCLUSIONS

The present paper is part of an ongoing investigation related to the optimal control of tentacle-like planar manipulators. The model, generalizing the Euler-Bernoulli beam, is discussed here in the stationary case. We focused on the problem to find optimal configurations of the manipulator touching some prescribed points on the boundary of an obstacle, while minimizing a quadratic cost on the curvature controls. The numerical tests confirm the consistency and applicability of our theoretical approach.

We regard at these results as a preliminary step towards optimal grasping problems. More precisely, here we addressed the problem to touch a finite set of fixed target points (while avoiding an obstacle and optimizing the shape of the manipulator). Our next step will be to select among the boundary of a target object, those (four) optimal target points ensuring planar force closure conditions. The goal of a forthcoming investigation is indeed to optimize both the target points as well as the contact sub-region of the manipulator and the associated controls, in order to get a steady, optimal grasp of a planar object.

REFERENCES

Bobrow, J. E., Dubowsky, S., and Gibson, J. (1983). On the optimal control of robotic manipulators with actuator constraints. In *1983 American Control Conference*, pages 782–787. IEEE.

Cacace, S., Lai, A. C., and Loreti, P. (2019a). Control strategies for an octopus-like soft manipulator. In *Proceedings of the 16th International Conference on Informatics in Control, Automation and Robotics - Volume 1: ICINCO,*, pages 82–90. INSTICC, SciTePress.

Cacace, S., Lai, A. C., and Loreti, P. (2019b). Optimal reachability and grasping for a soft manipulator. In *International Conference on Informatics in Control, Automation and Robotics*, pages 16–34. Springer.

Cacace, S., Lai, A. C., and Loreti, P. (2020a). Modeling and optimal control of an octopus tentacle. *SIAM Journal on Control and Optimization*, 58(1):59–84.

Cacace, S., Lai, A. C., and Loreti, P. (2020b). Optimal reachability with obstacle avoidance for hyper-redundant and soft manipulators. In *ICINCO 2020 - Proceedings of the 17th International Conference on Informatics in Control, Automation and Robotics*, pages 134–141.

Cacace, S., Lai, A. C., and Loreti, P. (2021). Constrained reachability problems for a planar manipulator. *arXiv preprint, arXiv:2101.08149*.

Christian Kanzow, D. S. and Wachsmuth, D. (2018). An augmented lagrangian method for optimization problems in banach spaces. *SIAM Journal on Control and Optimization*, 56(1):272 – 291.
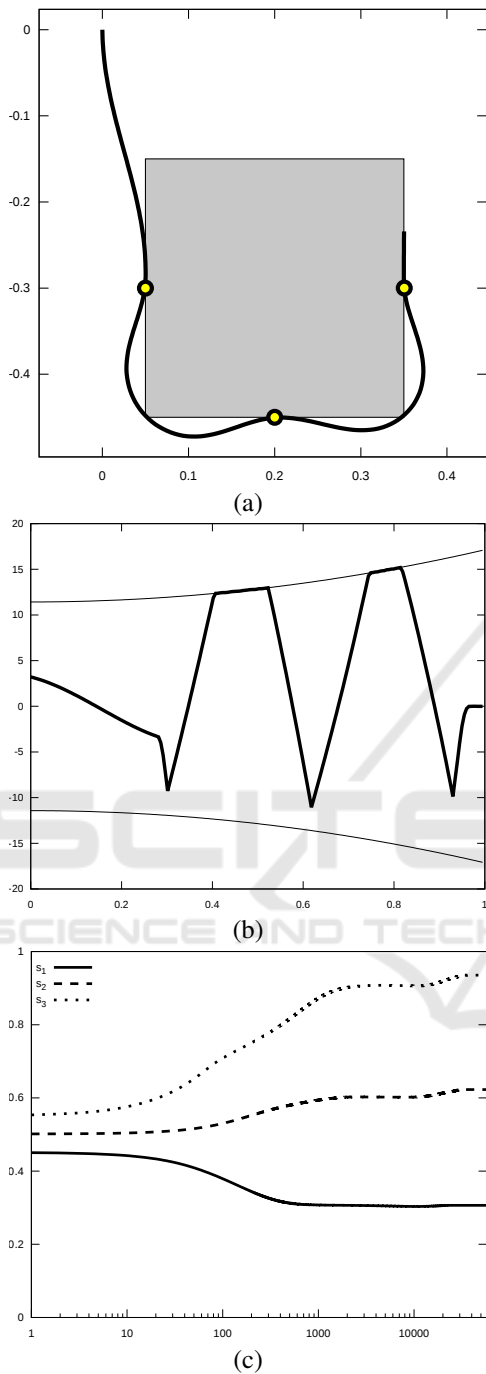
Figure 7: Test 7, optimal configuration (a), optimal curvature (b), and convergence history of the optimal contact points (c).

avoid the bottom corners of the obstacle, the manipulator is forced to push its curvature up to the threshold $\bar{\omega}$ on two quite large intervals.

George Thuruthel, T., Ansari, Y., Falotico, E., and Laschi, C. (2018). Control strategies for soft robotic manipulators: A survey. *Soft robotics*, 5(2):149–163.

Hestenes, M. (1969). Multiplier and gradient methods. *Journal of Optimization Theory and Applications*, 4:303–320.

Hughes, J., Culha, U., Giardina, F., Guenther, F., Rosendo, A., and Iida, F. (2016). Soft manipulators and grippers: A review. *Frontiers in Robotics and AI*, 3:69.

Jones, B. A. and Walker, I. D. (2006). Kinematics for multisection continuum robots. *IEEE Transactions on Robotics*, 22(1):43–55.

Kang, R., Kazakidi, A., Guglielmino, E., Branson, D. T., Tsakiris, D. P., Ekaterinaris, J. A., and Caldwell, D. G. (2011). Dynamic model of a hyper-redundant, octopus-like manipulator for underwater applications. In *Intelligent Robots and Systems (IROS), 2011 IEEE/RSJ International Conference on*, pages 4054–4059. IEEE.

Lai, A. C. and Loreti, P. (2014). Robot's hand and expansions in non-integer bases. *Discrete Mathematics & Theoretical Computer Science*, 16(1).

Lai, A. C., Loreti, P., and Vellucci, P. (2016). A fibonacci control system with application to hyper-redundant manipulators. *Mathematics of Control, Signals, and Systems*, 28(2):15.

Laschi, C. and Cianchetti, M. (2014). Soft robotics: new perspectives for robot bodyware and control. *Frontiers in bioengineering and biotechnology*, 2:3.

Laschi, C., Cianchetti, M., Mazzolai, B., Margheri, L., Follador, M., and Dario, P. (2012). Soft robot arm inspired by the octopus. *Advanced Robotics*, 26(7):709–727.

Michalak, K., Filipiak, P., and Lipinski, P. (2014). Multiobjective dynamic constrained evolutionary algorithm for control of a multi-segment articulated manipulator. In *International Conference on Intelligent Data Engineering and Automated Learning*, pages 199–206. Springer.

Powell, M. (1969). *A method for nonlinear constraints in minimization problems*. Academic Press, New York, NY.

Rus, D. and Tolley, M. T. (2015). Design, fabrication and control of soft robots. *Nature*, 521(7553):467–475.

Wang, B., Wang, J., Zhang, L., Zhang, B., and Li, X. (2016). Cooperative control of heterogeneous uncertain dynamical networks: An adaptive explicit synchronization framework. *IEEE transactions on cybernetics*, 47(6):1484–1495.